# SWARM INTELLIGENCE-BASED TECHNIQUE TO ENHANCE PERFORMANCE OF ANN IN STRUCTURAL DAMAGE DETECTION

**Ho Viet Long, Trinh Thi Trang, Ho Xuan Ba**[*]

Campus in Ho Chi Minh City, University of Transport and Communications, No 450-451 Le Van Viet Street, Ho Chi Minh, Vietnam

[*] *Corresponding author*
Email: bahx_ph@utc.edu.vn

**Abstract.** Artificial neural network (ANN), a powerful technique, has been used widely over the last decades in many scientific fields including engineering problems. However, the backpropagation algorithm in ANN is based on a gradient descent approach. Therefore, ANN shows high potential in local stagnancy. Besides, choosing the right architecture of ANN for a specific issue is not an easy task to deal with. This paper introduces a simple, effective hybrid approach between an optimization algorithm and a traditional ANN for damage detection. The global search-ability of a heuristic optimization algorithm, namely grey wolf optimizer (GWO), can solve the drawbacks of ANN and also improve the performance of ANN. Firstly, the grey wolf optimizer is used to update the finite element (FE) model of a laboratory steel beam based on the vibration measurement. The updated FE model of the tested beam then is used to generate data for network training. For an effective training process, GWO is utilized to identify the optimal parameters for ANN, such as the number of the hidden nodes, the proportion of dataset for training, validation, test, and the training function. The optimization process provides an optimal structure of ANN that can be used to predict the damages in the beam. The obtained results confirm the accuracy, effectiveness, and reliability of the proposed approach in (1) alleviating the differences between measurement and simulation and (2) damage identification including damage location and severity, in the tested beam considering noise effects. For both applications, dynamic characteristics like natural frequencies and mode shapes of the beam derived from the updated FE model, are collected to calculate the objective function.

**Keywords:** model updating, grey wolf optimizer, artificial neural network, hybrid approach, modal flexibility, damage identification.

## 1. INTRODUCTION

The most effective way to prevent unexpected failures of structures is to develop an assessment tool that can predict their health status timely. The presence of damages in structures can cause changes in modal properties. Therefore, these dynamic properties are efficient parameters in damage detection. These characteristics can be easily obtained under ambient excitation with low-cost and simple operation [1-4]. However, vibration measurement always faces up to noise that contaminates the collected data. Unpure data can lead to misidentifying the location as well as the quantity of damage. This reduces the effectiveness of using the modal properties.

An artificial intelligence-based approach inspired by the natural structure of the human brain is a powerful tool to solve this problem. The application of this approach is very diverse such as prediction, classification or estimation [5-6]. Seguini *et al*. successfully employed ANN and Particle Swarm Optimization (PSO) in crack prediction in the pipeline [7]. They aimed to enhance the performance of ANN by means of identifying the best weights and biases. In studies [8-9], Khatir *et al*. proposed a combination of optimization algorithms and ANN, to identify the damage severity based on damage indices e.g. Cornwell indicator, modal strain energy. Ho *et al.* [10] utilized a hybrid algorithm particle swarm optimization – gravitational search algorithm (PSOGSA), to improve Feedforward neural network (FNN) based on the optimal training parameters (weights and biases). Quantification of damage in a steel plate was the main aim of this study. Tran-Ngoc *et al.* combined ANN and Cuckoo search to obtain the best training parameters for damage detection in beam-like structures and a truss bridge [11]. Trapping in local minima is the main shortcoming of ANN. Authors in [12] developed a new method that combines genetic algorithm (GA) - Cuckoo search (CS) and ANN, namely ANNHGACS, to avoid local stagnation. In this approach, the hybrid evolutionary algorithm and ANN work parallel during the network training process. The success of damage detection in laminated composite structures confirmed its feasibility in practical application.

Almost the above studies did not focus on the size of the hidden layer in ANN. As we know, the size of input and output layers can be identified based on the data used. However, how many neurons should be used in a hidden layer for a specific problem is not easy to answer. Stated differently, choosing the number of nodes in each hidden layer is a crucial decision that can tremendously affect the performance of a neural network. Too many nodes or too few nodes in each hidden layer can cause overfitting and a time-consuming process or underfitting. In many cases, deciding the number of nodes in a hidden layer was based on experience or investigation of several numbers of hidden neurons. Some authors studied the optimal number of the hidden node for their problems [13-14]. However, there is not a consistent answer for the calculation of the optimal number of neurons in each hidden layer. Another matter in ANN is the proportion of data for training, validation, and test. Either less training data or less testing data can cause greater variance in estimated parameters. Some common data splits are 60-40, 70-30, 80-20, etc. The ratio of data division can be different depending on the specific problem, the amount of available dataset. Pauletto *et al*. proposed an optimal ANN for multicomponent adsorption by manually investigating several parameters e.g. activation function, training algorithm, number of hidden nodes [15]. In this study, they identified the optimal ANN based on mean squared error and *R*-values. It can be said that the approach to a creation of an optimal artificial neural network requires much effort, experience and time.

Therefore, this paper introduces a simple approach to obtain an optimal ANN based on calculation instead of experience or manual investigation. The core of the proposed method is the global search-ability of a heuristic optimization algorithm, namely grey wolf optimizer (GWO) [16]. Stochastic techniques in GWO is employed to determine the best value of training parameter e.g. the number of hidden neurons, data proportion, and training function based on the obtained mean squared error (MSE).

The paper consists of four sections. The introduction is in the first section. The next section is the methodology of the proposed method GWOANN. Section 3 is the case study that uses GWO for model updating of a laboratory steel beam and improves the training process of ANN for damage detection. The last section claims the highlight conclusions.

## 2. GWO-ANN METHODOLOGY

### 2.1. Grey wolf optimizer GWO

The hunting behaviour and social hierarchy of grey wolves are the inspirations of grey wolf optimizer (GWO) [16]. In their social hierarchy, the three top wolves i.e. wolf $\alpha$, $\beta$, $\delta$ representing the three best solutions, lead the pack in hunting preys. Encircling prey is described in a mathematical form:

$$\vec{D} = \left| \vec{C} \times \vec{X}_p(iter) - \vec{X}(iter) \right| \tag{1}$$

$$\vec{X}(iter+1) = \vec{X}_p(iter) - \vec{A} \times \vec{D} \tag{2}$$

$\vec{X}_p(iter)$, $\vec{X}(iter)$ represent the vector of wolf and prey's positions at the current iteration $iter$. The two coefficient vectors $\vec{A}, \vec{C}$ can be computed based on two random vectors $\vec{r}_1$, $\vec{r}_2$ in an interval [0 1] and the max number of iteration $iter_{max}$:

$$\vec{A} = 2 \times \vec{a} \times \vec{r}_1 - \vec{a} \tag{3}$$

$$\vec{a} = 2 \times \left( 1 - \frac{iter}{iter_{max}} \right) \tag{4}$$

$$\vec{C} = 2 \times \vec{r}_2 \tag{5}$$

In GWO, the search agents' positions are updated based on the positions of the three best search agents. Therefore, the three best solutions in the search space are stored in each iteration. Eqs. (1), (2) are rewritten concerning the three wolves $\alpha$, $\beta$, and $\delta$:

$$\vec{D}_{\alpha/\beta/\delta} = \left| \vec{C}_{1/2/3} \times \vec{X}_{\alpha/\beta/\delta} - \vec{X} \right| \tag{6}$$

$$\vec{X}_{1/2/3} = \vec{X}_{\alpha/\beta/\delta} - \vec{A}_{1/2/3} \times \vec{D}_{\alpha/\beta/\delta} \tag{7}$$

A new position of each wolf in the next iteration can be identified as follows:

$$\vec{X}(iter+1) = \frac{\vec{X}_1 + \vec{X}_2 + \vec{X}_3}{3} \tag{8}$$

It can be observed that the three wolves $\alpha$, $\beta$, and $\delta$ try to locate the prey's position and the positions of other wolves can be randomly updated around the prey.
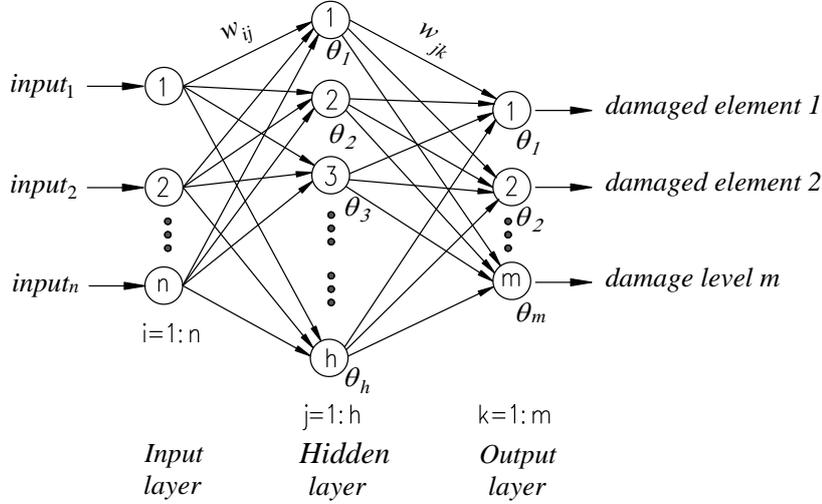
## 2.2. How does GWO-ANN work



Figure 1. An architecture of ANN.

Figure 1 shows an ANN's structure for damage identification consisting of one input layer, one hidden layer and one output layer. Weights $w_{ij}$ implies the connection between the input node $i^{th}$ and hidden node $j^{th}$ while $w_{jk}$ represents the connection between the hidden node $j^{th}$ and output node $k^{th}$. The biases at node $j^{th}$ in the hidden layer and node $k^{th}$ in the output layer are $\theta_j$ and $\theta_k$.

In this study, a suitable structure of ANN can be obtained by trial and error. Training with the known inputs and outputs is carried out by using an optimization algorithm, GWO. The step-by-step operation of GWOANN is introduced as in Figure 2.

From the below flowchart, unknown parameters e.g. the number of hidden nodes, data split, and training function, are input to GWO as variables. Then ANN is used to calculate the fitness of every individual wolf. Next, these fitness values are used to identify the top three wolves $\alpha$, $\beta$, and $\delta$. All search agents' positions are updated until meeting the stop condition i.e. either the current iteration greater than the max number of iteration or the best fitness is less than $10^{-6}$. During the optimization process, GWOANN tries to minimize the value of the fitness function as calculated:

$$objective\ function = MSE = \frac{1}{n}\sum_{z=1}^{n}\left(Y^{z}_{predicted} - Y^{z}_{target}\right)^{2} \tag{9}$$

where $n$ is the total number of data samples, $Y^{z}_{predicted}$ and $Y^{z}_{target}$ imply the predicted and target values when training data $z^{th}$ is used, respectively.
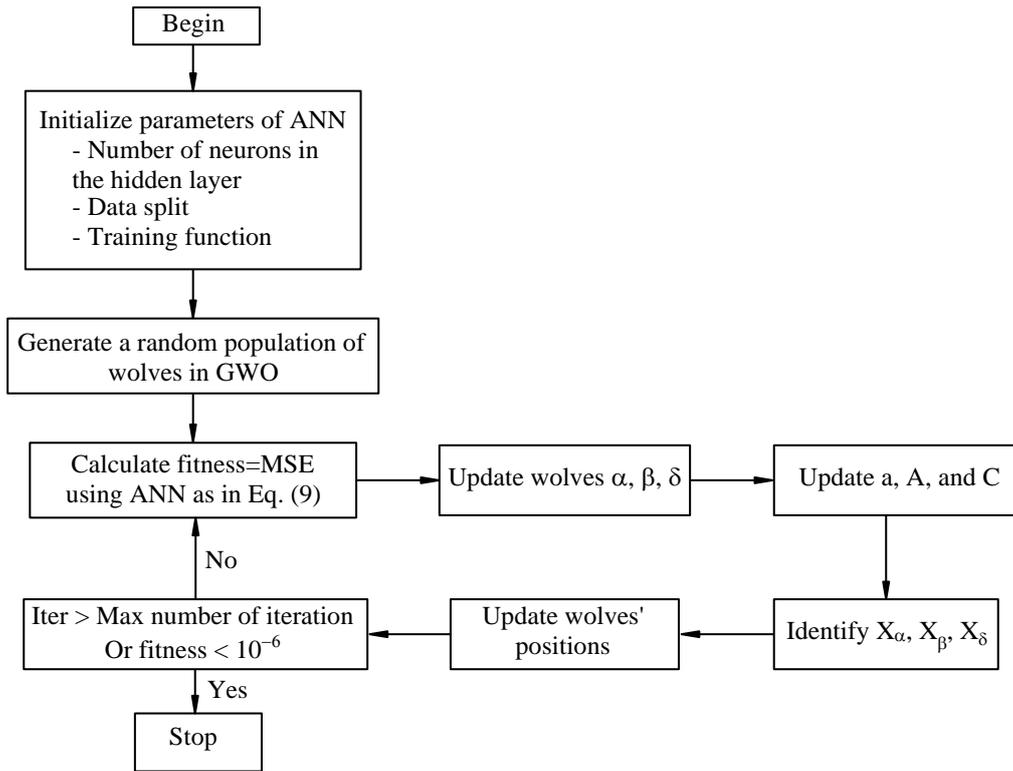
Figure 2. Flowchart of GWOANN's working procedure.

## 3. CASE STUDY

### 3.1. Experimental description

The vibration of a laboratory beam with a free-free condition is the objective of this study. Geometrical dimensions of the beam are $L \times b \times h = 1 \times 0.07 \times 0.0096$ (*m*) with *L*, *b*, and *h* are the length, width, and height of the beam, respectively. The above dimension is an average value using measured values at 15 positions as in Figure 3a.

In the first step, the dynamic properties of the beam are employed to build an FE model based on the inverse problem. In the second step, the updated FE model is assumed to suffer damage scenarios with various elements and severities. The generated data is collected and served in damage identification.

The measurement grid involved 30 points which were arranged along the beam. Three setups were used to cover all these points. One setup included 16 accelerometers with 8 sensors were served as reference points, and the others were roving points. These setups were connected by reference points i.e. the underlined and red numbers (see Figure 3a). The sampling rate was 2651 *Hz,* and the recording time was 300 seconds.

On-site sensor placement is displayed as in Figure 3b. A hammer struck the considered beam to create excitation. Free vibration of the beam was collected and treated by an output-only technic, namely covariance stochastic subspace identification (COV-SSI) [17]. Modal properties of the beam e.g. natural frequencies and mode shapes then were identified as in Table 1 and Figure 4.
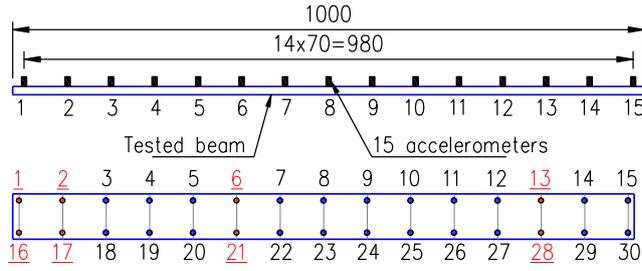
a. Entire measurement points on the beam

b. Using 16 accelerometers in one setup

Figure 3. Details of sensor placement.

Table 1. Summary of natural frequencies of the first six modes.

| Mode | Frequencies, $f$ (Hz) | Mode type |
|:---:|:---:|:---:|
| **1** | 50.79 | Vertical bending |
| **2** | 140.11 | Vertical bending |
| **3** | 273.12 | Vertical bending |
| **4** | 454.76 | Vertical bending |
| **5** | 677.31 | Vertical bending |
| **6** | 947.12 | Vertical bending |



1st mode, $f_1$=50.79 Hz

2nd mode, $f_2$=140.11 Hz

3rd mode, $f_3$=273.12 Hz

4th mode, $f_4$=454.76 Hz

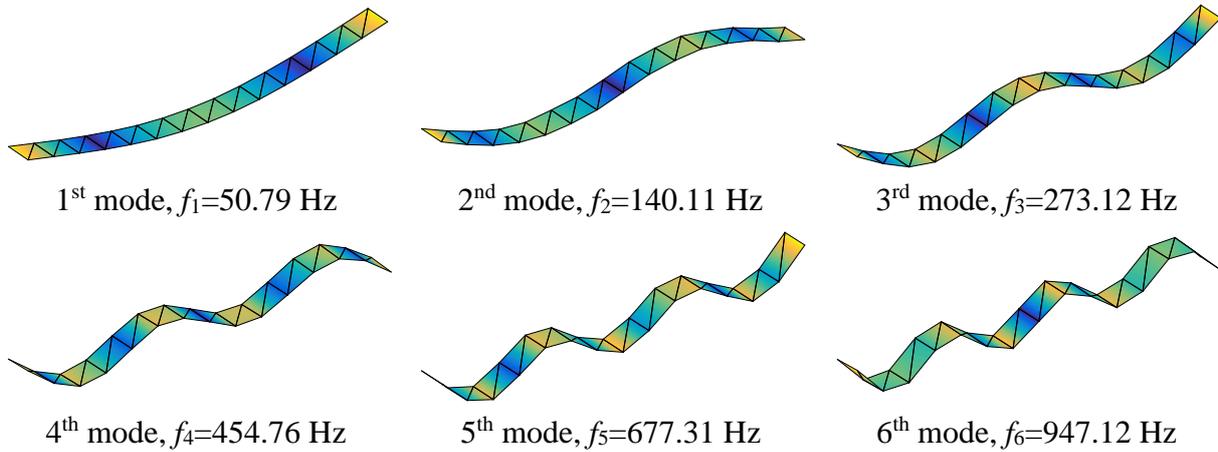5th mode, $f_5$=677.31 Hz

6th mode, $f_6$=947.12 Hz

Figure 4. The first six modes obtained from the measurement.

### 3.2. Initial numerical model and model updating

#### a. Initial FE model

A FE model was built in ANSYS [18] to perform the dynamic behaviour of the tested beam based on vibration measurement. In the initial FE model, sixteen SHELL181 elements were employed to model the beam with a free-free boundary condition. The initial material properties: Young's modulus $E$=2×10$^{11}$$Mpa$, density $\rho$=7800 $kg/m^3$, Poisson's ratio $v = 0.3$ were used for the FE model.

1ˢᵗ mode, $f_1$=49.97 Hz          2ⁿᵈ mode, $f_2$=137.74 Hz          3ʳᵈ mode, $f_3$=270.06 Hz

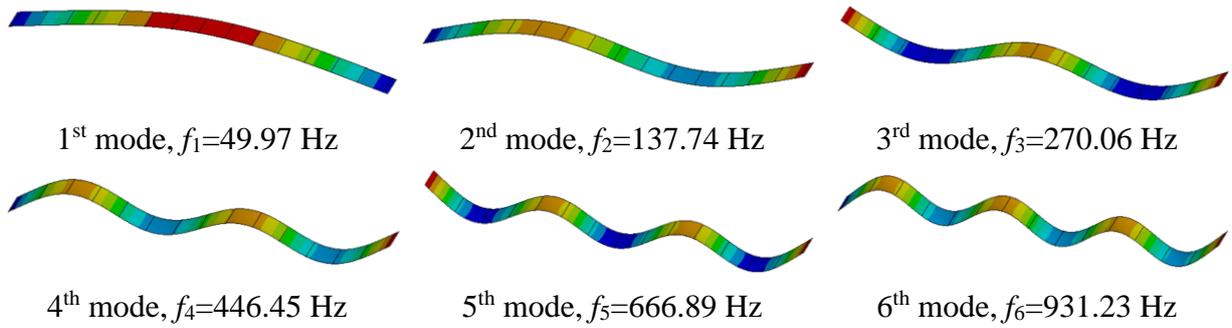4ᵗʰ mode, $f_4$=446.45 Hz          5ᵗʰ mode, $f_5$=666.89 Hz          6ᵗʰ mode, $f_6$=931.23 Hz

Figure 5. The first six modes obtained from the initial FE model.

The first six modes were extracted from the initial FE model. Figure 5 are the obtained modes from dynamic analysis. In Table 2, the differences in frequencies between simulation and measurement are less than 1.83% for all considered modes. However, these deviations should be reduced before the FE model can be used as a baseline model for damage detection.

Table 2. Calculated and measured frequencies.

| Mode | Frequencies, $f$ (Hz) | | Error$_{Initial}$ [1] |
|---|---|---|---|
| | Measurement | Initial FE | (%) |
| 1 | 50.79 | 49.97 | 1.61 |
| 2 | 140.11 | 137.74 | 1.69 |
| 3 | 273.12 | 270.06 | 1.12 |
| 4 | 454.76 | 446.45 | 1.83 |
| 5 | 677.31 | 666.89 | 1.54 |
| 6 | 947.12 | 931.23 | 1.68 |

### b. Model Updating

Underestimated stiffness and manufacturing imperfection of the beam, weights of sensors could cause discrepancies in frequencies between the initial FE and measurement. Therefore, these effects were taken into account via 17 updating parameters with one Young's modulus and 16 densities concerning 16 elements in the model, as shown in Table 3.

Table 3. Uncertain parameters in the initial FE model.

| Updating parameters | Lower bound | Upper bound |
|---|---|---|
| Young's modulus, E | $1.9 \times 10^{11}$ | $2.1 \times 10^{11}$ |
| Density, $\rho_e$ with $e$=1 to 16 | 7750 | 8050 |

All these parameters were treated as variables in an optimization process using GWO. The objective function was calculated using the changes in frequencies and mode shapes as follows:

---

[1] Error$_{Initial}$ = (Measurement − Initial FE)×100/Measurement

$$Objective\ function = \sum_{q=1}^{M}\left(1 - \frac{f_q^{calculated} \times f_q^{measured}}{\left(f_q^{measured}\right)^2}\right)^2 + \sum_{q=1}^{M}\left(1 - MAC_{q,q}\right)^2 \qquad (10)$$

Where $M$ is the number of considered modes, $f_q^{calculated}$, $f_q^{measured}$ imply numerical and experimental frequencies regarding mode $q^{th}$, $MAC_{q,q}$ indicates diagonal values of $MAC$ matrix that was identified as:

$$[MAC] = \left[\frac{|\sum_{p=1}^{N}(\phi_{p,q}^{measured})^T \times (\phi_{p,q}^{calculated})|^2}{\left(\sum_{p=1}^{N}(\phi_{p,q}^{measured})^T \times (\phi_{p,q}^{measured})\right) \times \left(\sum_{p=1}^{N}(\phi_{p,q}^{calculated})^T \times (\phi_{p,q}^{calculated})\right)}\right] \qquad (11)$$

Where $N=15$, is the number of considered nodes, $\phi_{p,q}^{measured}$, $\phi_{p,q}^{calculated}$ are measured and calculated displacement mode shapes at node $p^{th}$ in mode $q^{th}$, $^T$ is the transposition.
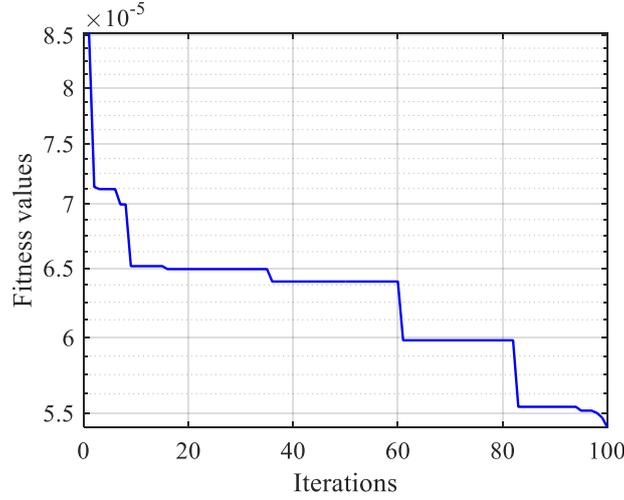


Figure 6. The evolutionary curve of fitness values using GWO.

GWO was employed to minimize the objective function until meeting a stopping condition, the current iteration greater than the max number of iteration or the best fitness is less than $10^{-6}$. In this case, some parameters for GWO e.g. population 50, iteration 100 were chosen. Modal properties of the first six modes were utilized to compute the objective function as in eq. (10). After 100 iterations, the convergence curve of fitness values is plotted in Figure 6. The best fitness value is less than $5.5 \times 10^{-5}$. This guarantees a good match between simulation and measurement.

Table 4. The obtained uncertainties after updating.

| $\rho_1$ | $\rho_2$ | $\rho_3$ | $\rho_4$ | $\rho_5$ | $\rho_6$ | $\rho_7$ | $\rho_8$ | $E$ |
|------|------|------|------|------|------|------|------|------|
| 8031 | 7896 | 7750 | 8009 | 7885 | 7933 | 7750 | 8050 | |
| $\rho_9$ | $\rho_{10}$ | $\rho_{11}$ | $\rho_{12}$ | $\rho_{13}$ | $\rho_{14}$ | $\rho_{15}$ | $\rho_{16}$ | $2.1 \times 10^{11}$ |
| 8050 | 7750 | 7820 | 8050 | 7953 | 8002 | 8012 | 7959 | |

Table 5. Updated frequencies.

| Mode | Frequencies, $f$ ($Hz$) | | | Error$_{Updated}$ [2] (%) | MAC |
|---|---|---|---|---|---|
| | Measurement | Initial FE | Updated FE | | |
| 1 | 50.79 | 49.97 | 50.77 | −0.04 | 0.999 |
| 2 | 140.11 | 137.74 | 140.11 | 0.00 | 0.994 |
| 3 | 273.12 | 270.06 | 273.76 | 0.23 | 0.999 |
| 4 | 454.76 | 446.45 | 454.56 | −0.04 | 0.998 |
| 5 | 677.31 | 666.89 | 677.49 | 0.03 | 0.999 |
| 6 | 947.12 | 931.23 | 947.29 | 0.02 | 0.997 |

The updated parameters in Table 4, then were input to the FE model to recalculate modal characteristics. Table 5 indicates that the maximum error between simulation and experiment is significantly decreased from 1.83% to under 0.23%. All MAC values are higher than 0.994. These confirm that the updated FE model can perform similar behaviour compared with the real one. Stated differently, the updated FE model can be considered as a baseline model that is used for defect identification.

## 3.3. Damage detection using GWOANN

In this section, several multiple damage scenarios with white Gaussian noise are used to evaluate the proposed approach GWOANN compared to the traditional ANN. MSE, error histogram and regression R-values are the comparative objectives.
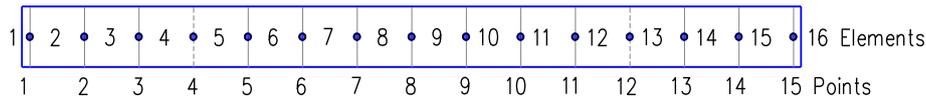
*a. Damage scenarios and damage index*



Figure 7. Element label on the updated FE model.

This study aims to investigate the ability of a hybrid method in identifying the optimal number of hidden neurons, data division and training function for ANN. To reduce the computational time, two elements among 5 to 12 were assumed to be damaged with the same level from 1 to 50% at an interval of 1%. There were $N_{samples} = 50 \times C_8^2 = 50 \times 28 = 1400$ samples.

Table 6. The assumed damaged elements and corresponding levels.

| Scenarios | Element 1 | Element 2 | Stiffness reduction (%) |
|---|---|---|---|
| 1 | 6 | 7 | 35.5 |
| 2 | 6 | 8 | 30.5 |
| 3 | 6 | 10 | 33.4 |
| 4 | 7 | 11 | 32.5 |
| 5 | 8 | 10 | 25.3 |
| 6 | 9 | 11 | 37.5 |

---

[2] Error$_{Updated}$ = (Updated FE − Measurement)×100/Measurement

Besides, several extra damage scenarios were generated to evaluate the trained network in Table 6. The dynamic properties of the healthy and unhealthy beam were added white Gaussian noise with signal-to-noise ratio, *snr* = 50 *dB*. These dynamic properties were collected to calculate the damage index.

In this study, modal flexibility index was chosen as the damage indicator due to its sensitivity to damages when a few lower modes obtained [19]. The flexibility matrices of healthy and unhealthy structures, $MF_H$ and $MF_{UH}$ are calculated:

$$MF_H = \left[\sum_{q=1}^{M} \frac{1}{f_q^2} \Phi_{p,q}.\Phi_{p,q}^T\right]_H \tag{12}$$

$$MF_{UH} = \left[\sum_{q=1}^{M} \frac{1}{f_q^2} \Phi_{p,q}.\Phi_{p,q}^T\right]_{UH} \tag{13}$$

where M is the number of investigated modes, $\Phi_{p,q}$ indicates mass-normalized mode shape of mode $q^{th}$, $f_q$ natural frequency in mode $q^{th}$, superscript $^T$ implies transposition.

Changes in the flexibility matrices between damaged and undamaged structures are as follows:

$$\Delta MF = MF_{UH} - MF_H \tag{14}$$

The damage index at location $p^{th}$ is the maximum absolute values of each column in $\Delta MF$ matrix:

$$\Delta MF_p = \max\left|\Delta MF_{column\ p}\right| \tag{15}$$

Figure 8 is an illustration of the damage index $\Delta MF$ along the beam in two damage cases. In the first case, two elements 6 and 8 are assumed to be decreased stiffness by 30%. A stiffness reduction of 15% in two elements 7 and 10 is considered in the second case. In each case, damage indices at 15 points (labelled in Figure 7), damaged elements and corresponding extent are collected to generate data training in the next section. In this study, 15 neurons in the input layer consist of values of damage indices at 15 points. The output layer includes three neurons that represent two labels of defected elements and one severity. The summary table of input parameters and target outputs are shown in Table 7.
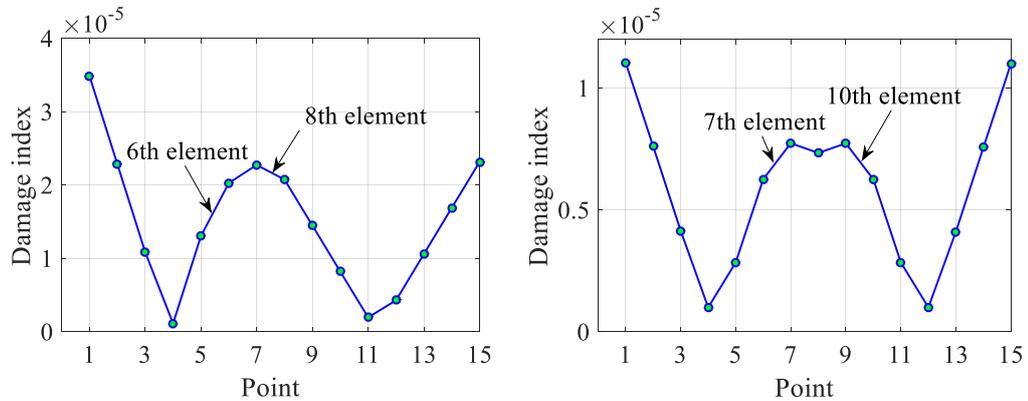


a. Case 1: Elements 6, 8 / 30%            b. Case 2: Elements 7, 10 / 15%

Figure 8. Maximum absolute flexibility change index at 15 points along the observed beam.

*b. The architecture of the neural network*

Some pre-set parameters for the traditional ANN were: $2/3 \times I_{nodes} + O_{nodes} = 13$ hidden nodes [20-21], a common data division 70-15-15 for training, validation and test, using train function Levenberg Marquardt (trainlm). In contrast, GWOANN identified all these parameters based on an optimization process. Several training functions [15] e.g. Levenberg-Marquardt (trainlm), BFGS quasi-Newton (trainbfg), Scaled conjugate gradient (trainscg), Gradient descent with momentum and adaptive learning rate (trainingdx), and Resilient backpropagation (trainrp), are investigated its effectiveness for this problem. Bayesian Regulation (trainbr) was not used in this study due to its computational cost.

Table 7. Details of ANN's architecture.

| Method | Input nodes | Hidden nodes | Output nodes | Training Function |
|---|---|---|---|---|
| **ANN** | 15 | 13 | 3 | Trainlm |
| **GWOANN** | 15 | $H_{nodes} \in [1 - 30]$ | 3 | The best one from "trainlm, trainbfg, trainscg, trainingdx, trainrp" |

Authors in [20] also mentioned that the size of the hidden layer should be less than twice input neurons. Therefore, an interval of the number of hidden neurons from 1 to $2 \times I_{nodes} = 30$ was used to avoid overfitting and reduce the computational time. Data samples for training varied from 50 to 80% of the total samples. The data for validation and test was equally divided based on the identified data samples for training.

*c. Results*

An optimization process was conducted by GWO with population 40, iteration 50. After 4098 seconds, the convergence curve of the best fitness during 50 iterations are plotted as in Figure 9. The best value of the fitness function (MSE) is quickly converged after 6 iterations then levelling off. The optimal architecture of ANN is 15-19-3, using an 80-10-10 split and trainlm as the training function.
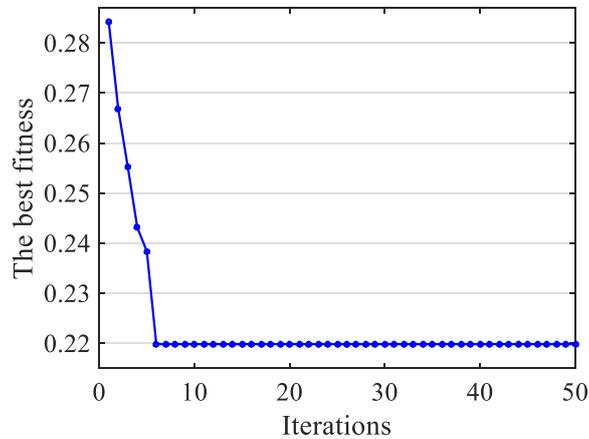


Figure 9. The fitness convergence curve using GWOANN.

Table 8. Performance indices of ANN and GWOANN for multiple damage scenarios.

| Method | MSE | $R$ values |
|--------|-----|-----------|
| ANN | 0.3318 | 0.99879 |
| GWOANN | 0.2198 | 0.9992 |

Figure 10 indicates that a superior agreement between the target and predicted values using two methods. The dataset of training, validation, and test, is distributed along a 45-degree line. $R$-values for all cases using GWOANN are improved in comparison with using ANN. Besides, the mean squared error (MSE) obtained by GWOANN is also lower than that of ANN (Table 8)
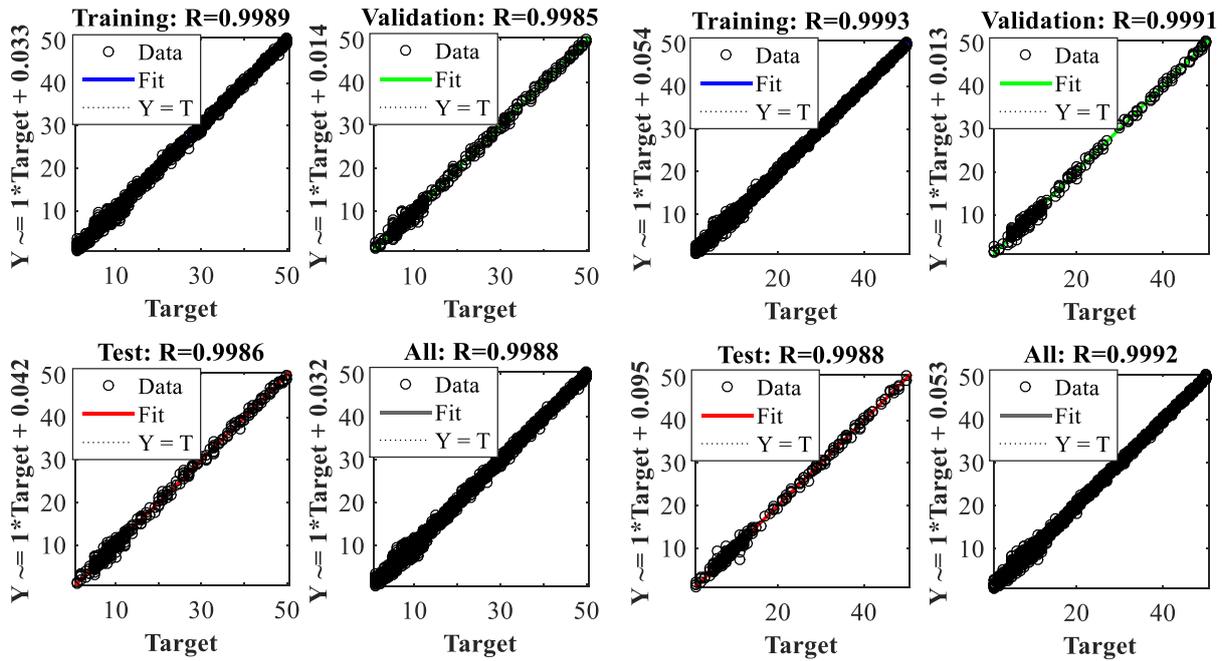


a. Using ANN                         b. Using GWOANN

Figure 10. Regression plots (Y and T are Output and Target)
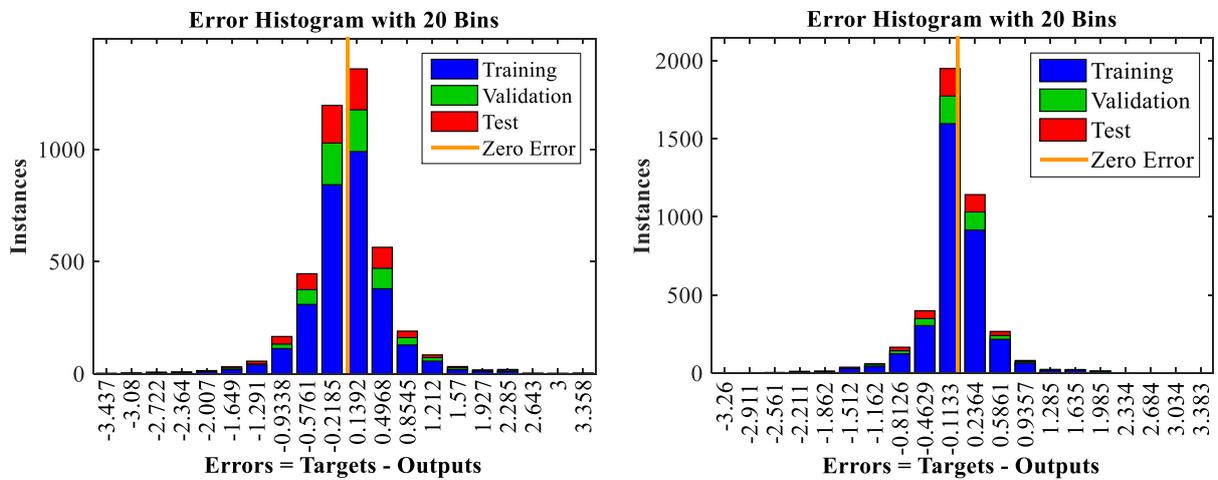


a. Using ANN                         b. Using GWOANN

Figure 11. Error histogram.

Errors between the predicted and target values are depicted on the error histogram (see Figure 11). It can be observed that GWOANN has much more errors that spread around the zero error value in comparison with using ANN. From all the discussed points, GWOANN is able to identify a better structure for ANN using an optimization procedure.

The obtained optimal structure of ANN then was used for damage localization and quantification using unlearnt data from damage scenarios in Table 6. Damage identifications are plotted in Figure 12. Both methods can exactly predict the damaged elements. Due to the high noise mentioned above, there are slight differences between the observed and estimated severities. Details of the identified extent of damage are shown in Table 9. Only the predicted value by ANN in the first case shows a better agreement with the desired value over using GWOANN (see Figure 12a). It can be seen that the deviation in the predicted levels between ANN and GWOANN is very low, 0.04%. Both methods perform the same prediction in the third case (see Figure 12c). The other cases reveal that the performance of GWOANN is better than that of ANN (see Figure 12b,d-e). Generally speaking, most of the predictions using GWOANN are closer to the actual damage levels compared with ANN. This result once again confirms the feasibility and effectiveness of GWOANN in improving the performance of ANN.
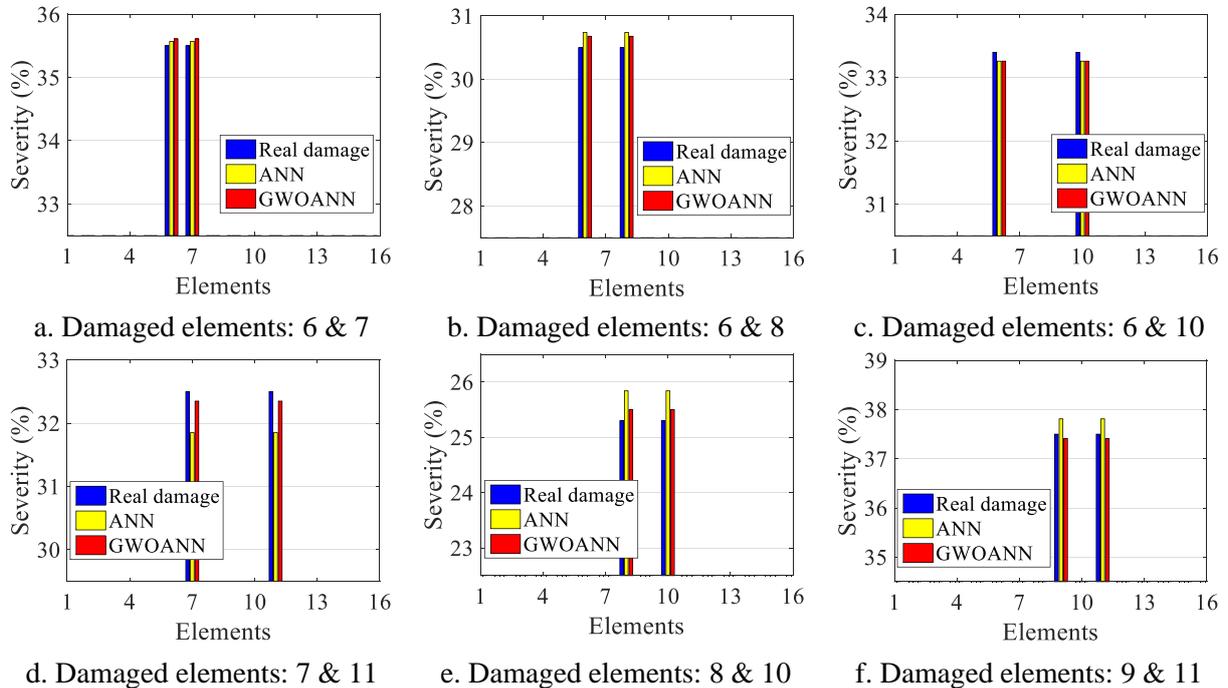
a. Damaged elements: 6 & 7    b. Damaged elements: 6 & 8    c. Damaged elements: 6 & 10

d. Damaged elements: 7 & 11    e. Damaged elements: 8 & 10    f. Damaged elements: 9 & 11

Figure 12.  Results of multiple damage detection using ANN, GWOANN.

Table 9. Results of damage quantification.

| Damage level | Damage scenarios | | | | | |
|---|---|---|---|---|---|---|
| (%) | CS1 | CS2 | CS3 | CS4 | CS5 | CS6 |
| **Desired value** | 35.5 | 30.5 | 33.4 | 32.5 | 25.3 | 37.5 |
| **Using ANN** | **35.57** | 30.74 | **33.26** | 31.85 | 25.84 | 37.81 |
| **Using GWOANN** | 35.61 | **30.68** | **33.26** | **32.35** | **25.5** | **37.41** |

## 4. CONCLUSION

This paper introduces an optimization-based approach that can be used effectively in structural damage detection with a simple implementation. The obtained results confirmed:

- Superior agreement between calculated and measured model is achieved by an optimization process using measurement data. The maximum discrepancies in frequencies are 0.23%, while the others less than 0.04%.

- A suitable architecture of ANN can be achieved based on an explicit calculation instead of the experience or perspective of an engineer.

- The achieved MSE, $R$-values, and error histogram are the obvious proofs that affirm the global search-ability of GWOANN in enhancing the performance of ANN

- The damaged elements can be exactly localized even white Gaussian noise contaminates the training data.

- The gap between actual and predicted damage levels is significantly alleviated by using GWOANN compared with ANN.

- Finally, the proposed approach generates a superior link between the damage index and damage quantification. This connection can not be obtained if using only the damage index.

The preliminary results open potential application of the proposed approach for damage detection in real structures.

## ACKNOWLEDGMENT

## REFERENCES

[1]. L. V. Ho, S. Khatir, G. D. Roeck, T. Bui-Tien, M. A. Wahab, Finite element model updating of a cable-stayed bridge using metaheuristic algorithms combined with Morris method for sensitivity analysis, Smart Structures And Systems, 26 (2020) 451–468. https://doi.org/10.12989/sss.2020.26.4.451

[2]. V. L. Ho, G. De Roeck, T. Bui-Tien, M. Abdel Wahab, Determination of the Effective Stiffness of Half-Open Cross-Section Bars and Orthotropic Steel Deck of a Truss Bridge Using Model Updating, in Proceedings of the 8th International Conference on Fracture, Fatigue and Wear, 2021, Springer, 97–108. https://doi.org/ 10.1007/978-981-15-9893-7_6

[3]. V. L. Ho, N. H. Tran, G. De Roeck, T. T. Bui, M. Abdel Wahab, System identification based on vibration testing of a steel I-beam, in Proceedings of the 1st International Conference on Numerical Modelling in Engineering, 20 (2019) 254–268. https://doi.org/10.1007/978-981-13-2405-5_21

[4]. D. T. Toan, Wireless DAQ using piezoelectric sensor for vibration measurement of bridge structure, Transport and communications science Journal, 2 (2020) 135-144. https://doi.org/10.25073/tcsj.71.2.8

[5]. N.T. Anh, L. H. Bang, Development of ANN-based models to predict the bond strength of GFRP bars and concrete beams, Transport and communications science Journal, 7 (2020) 814-827. https://doi.org/10.47869/tcsj.71.7.7

[6]. L. H. Bang, N. T. Anh, M. T. H. Van, Compressive strength prediction of recycled aggregate

concrete by artificial neural network, Transport and communications science Journal, 3 (2021) 369-383. https://doi.org/10.47869/tcsj.72.3.11

[7]. M. Seguini, S. Khatir, D. Boutchicha, D. Nedjar, M. A. Wahab, Crack prediction in pipeline using ANN-PSO based on numerical and experimental modal analysis, Smart Structures and Systems, 27 (2021) 507–523. https://doi.org/10.12989/SSS.2021.27.3.507

[8]. S. Khatir, S. Tiachacht, C.-L. Thanh, T. Q. Bui, M. Abdel Wahab, Damage assessment in composite laminates using ANN-PSO-IGA and Cornwell indicator, Composite Structures, 230 (2019) 111509. https://doi.org/10.1016/j.compstruct.2019.111509

[9]. S. Khatir *et al.*, An efficient hybrid TLBO-PSO-ANN for fast damage identification in steel beam structures using IGA, Smart Structures and Systems, 25 (2020) 605–617. https://doi.org/10.12989/SSS.2020.25.5.605

[10]. L. V. Ho, D. H. Nguyen, G. D. Roeck, T. Bui-Tien, M. A. Wahab, Damage detection in steel plates using feed-forward neural network coupled with hybrid particle swarm optimization and gravitational search algorithm, Journal of Zhejiang University-SCIENCE A (Applied Physics & Engineering), 22 (2021) 467-480. https://doi.org/10.1631/jzus.A2000316

[11]. H. Tran-Ngoc, S. Khatir, G. De Roeck, T. Bui-Tien, M. Abdel Wahab, An efficient artificial neural network for damage detection in bridges and beam-like structures by improving training parameters using cuckoo search algorithm, Engineering Structures, 199 (2019) 109637. https://doi.org/10.1016/j.engstruct.2019.109637

[12]. H. Tran-Ngoc, S. Khatir, H. Ho-Khac, G. De Roeck, T. Bui-Tien, M. Abdel Wahab, Efficient Artificial neural networks based on a hybrid metaheuristic optimization algorithm for damage detection in laminated composite structures, Composite Structures, 262 (2021) 113339. https://doi.org/10.1016/j.compstruct.2020.113339

[13]. K. G. Sheela, S. N. Deepa, Review on Methods to Fix Number of Hidden Neurons in Neural Networks, Mathematical Problems in Engineering, (2013) 1–11. https://doi.org/10.1155/2013/425740

[14]. J. Ke, X. Liu, Empirical Analysis of Optimal Hidden Neurons in Neural Network Modeling for Stock Prediction, in 2008 IEEE Pacific-Asia Workshop on Computational Intelligence and Industrial Application, Wuhan, China, (2008) 828–832. https://doi.org/10.1109/PACIIA.2008.363

[15]. P. S. Pauletto, G. L. Dotto, N. P. G. Salau, Optimal artificial neural network design for simultaneous modeling of multicomponent adsorption, Journal of Molecular Liquids, 320 (2020) 114418. https://doi.org/doi: 10.1016/j.molliq.2020.114418

[16]. S. Mirjalili, S. M. Mirjalili, A. Lewis, Grey Wolf Optimizer, Advances in Engineering Software, 69 (2014) 46–61. https://doi.org/10.1016/j.advengsoft.2013.12.007

[17]. MACEC 3.2: A Matlab toolbox for experimental and operational modal analysis, Belgium, 2011.

[18]. ANSYS, Inc. Southpointe, 275 Technology Drive, Canonsburg, PA 15317, Release 17.2, 2016.

[19]. A.K. Pandey, M. Biswas, Damage Detection in Structures Using Changes in Flexibility, Journal of Sound and Vibration, 169 (1994) 3-17. https://doi.org/10.1006/jsvi.1994.1002

[20]. Jeff Heaton, Introduction to Neural Networks for Java, 2nd Edition (2nd. ed.), Heaton Research, Inc, USA, 2008.

[21]. Z. Boger, P. O. Box, H. Guterman, Knowledge Extraction from Artificial Neural Networks Models, IEEE International Conference on Systems, Man, and Cybernetics. Computational Cybernetics and Simulation, 4 (1997) 3030–3035. https://doi.org/10.1109/ICSMC.1997.633051